

Hydrophobic and Hydrophilic Surfaces Created by Nanosecond Laser Structuring

Jeffrey M. Warrender

U.S. Army DEVCOM-Armaments Center, 1 Buffington St., Watervliet NY 12189

Corresponding author's email: jwarrend@post.harvard.edu

Steel and aluminum test panels were irradiated with large numbers of pulses from a Nd:YAG (532 nm) or KrF excimer (248 nm) at fluence between 0.3 and 3.0 J/cm², which induced changes to the surface topography of the panels. In most cases this led to considerable roughening of the surface, and decoration of the roughened surface with nanoscale particles. The contact angle of water droplets was measured, and showed both increased and decreased contact angle compared to unshot material, depending on the laser conditions. The changes to the surface hydrophobicity are non-monotonic in both laser fluence and shot density. Comparisons against surface topography suggest that the surfaces that exhibit two length scales of roughness are more likely to be excessively hydrophobic, whereas surfaces that have large scale features are more likely to be excessively hydrophilic.

DOI: 10.2961/jlmn.2022.03.2008

1. Introduction

Hydrophobic surfaces have attracted considerable scientific interest in recent years.¹⁻³ Surface topographical features are known in nature to exhibit superhydrophobicity, the classic example being the self-cleaning Lotus leaf.⁴⁻⁵ Engineered surfaces that exhibit the hydrophobic effect can modify the adhesion properties of the surface, with a key characteristic being the interaction of the *length scale* of the topographic features in comparison to the length scale of the features of the coating in question.⁶

In particular, laser irradiation has been shown to induce microstructural and chemical changes in the surfaces of both metallic and non-metallic materials, which can enhance their optical absorption⁷, tribological performance⁸, adhesion⁹, corrosion-resistance¹⁰⁻¹⁴, or hydrophobicity¹⁵⁻¹⁸. Many of these reports are for metal surfaces, but semiconductors⁷ and ceramics⁸ and polymeric materials⁹ are in view in some laser-modification studies. The effect that a laser will have on a given target is complicated, and depends on the laser's pulse duration and intensity, as well as on the initial microstructure and properties of the target. At low intensity, the laser may melt the surface, which can be used to induce surface alloying¹³ or to remove deleterious second-phase particles in alloyed metals¹¹. At higher instantaneous intensities, achieved with short pulse duration lasers, athermal processes begin to be important, and ejection of material via formation of a hot, dense plasma is observed. If performed in liquid, this creates shock waves that "peen" the surface, which can improve its corrosion resistance¹²; in air or in vacuum, ablation of material can lead to surface microstructures qualitatively described as "spikes" or "bumps", which improve hydrophobicity by reducing the ability of a water drop to spread out as it would on a flat metal surface.¹¹ Hydrophobic surfaces have attracted great attention in recent years as potential "self-cleaning" surfaces, with improved resistance to biological contamination, and the similar behavior of the small-scale (~10 micron) "protrusions" on the leaves of the Lotus plant inspire and motivate the search for similar behavior in metal substrates.¹⁶ For corrosion problems in which extended contact with hygroscopic substances is likely, improved

hydrophobicity may improve a coating's corrosion resistance as well.

Previous studies have reported on irradiations of steel and aluminum surfaces with femtosecond¹⁷⁻¹⁸, nanosecond^{9,11,14,15} and millisecond¹⁹ pulse durations. A systematic study of the effects of laser parameters on the surface morphology and hydrophobic behavior is presented here. The laser fluence, and the number of laser shots incident per unit area, are both systematically varied, and the resulting surfaces imaged in electron microscopy. Contact angle measurements show that for certain ranges of parameters, the surfaces become more hydrophobic, but in others they become more hydrophilic. Comparing morphology and contact angle data leads to the interpretation that the presence of two length scales are important for the emergence of a hydrophobic effect, consistent with the Lotus effect.

2. Experimental

Test panels of 3003-H14 aluminum and 4340 steel (Q-Labs Corp) were placed horizontally on a motorized stage and rastered under the focused beam of either a KrF laser (248 nm, 15 ns pulse) or a frequency-doubled Nd:YAG laser (532 nm, 6 ns pulse). The former produces a rectangular spot approximately 2 mm by 1 mm; the latter produces a circular spot 1.3 mm in diameter. The translation speed of the stage was varied, relative to the pulsing frequency of the laser, so as to controllably vary the average number of laser shots that would hit a given area of the sample. For each specimen, an area at least 0.25 cm² was irradiated. The output energy was varied so as to systematically vary the laser fluence

Nd:YAG irradiations were performed at 0.27, 1.15, and 2.3 J/cm². The shot densities were 80, 120, 310, and 820 shots per area. Excimer laser irradiations were performed at 0.3, 1.0, 1.5, and 3.0 J/cm². The shot densities were 375, 750, 1000, 1500, and 3000 shots per area.

The topography of the samples post-irradiation was examined with an electron microscope (FEI Helios Nanolab) at 20 kV, with measurements made in the secondary electron detector, at magnification from 350× to 35,000×.

The contact angle of a water droplet placed on the surface was measured with a contact angle meter (Attension), to determine the hydrophobicity of the

material pre- and post-irradiation. Unirradiated areas of each sample were measured as a control. Measurements were made with deionized water. The water was dropped onto the irradiated area and monitored with a camera for several seconds, then the surface was blown clean prior to the next droplet. The software fits the droplet image to a spherical cap to determine the contact angle. Each irradiated area was measured at least 3 times, and the measurements were averaged to determine the contact angle.

3. Results

In Fig. 1 and Fig. 2, we present contour plots for the contact angle after irradiation by excimer (Fig. 1) and Nd:YAG (Fig. 2), respectively. The contact angle for unshot material appears in the color bar for reference. As can be seen, both sets of excimer-irradiated samples show areas where the contact angle has increased, indicating that the surface has become more hydrophobic, and other regions where the contact angle has decreased, indicating that the surface has become more hydrophilic.

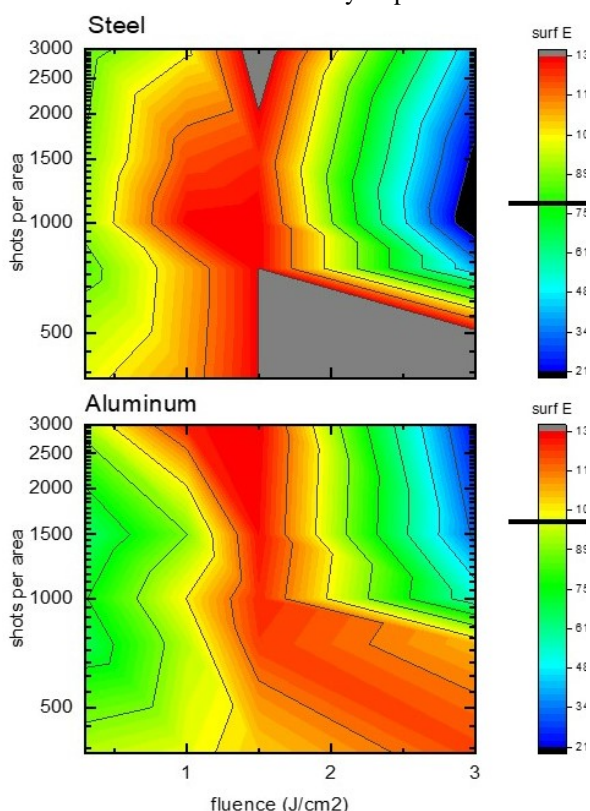


Fig. 1 Contact angle contour plot for steel (top) and aluminum (bottom) panels irradiated with a KrF excimer laser at varying laser fluence and shots per area. The black line shows the baseline contact angle for unirradiated material.

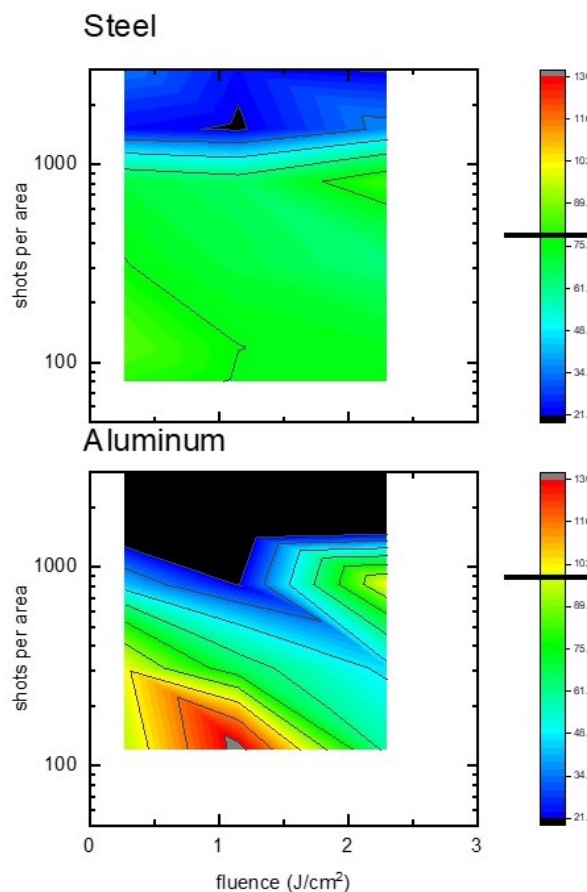


Fig. 2 Contact angle contour plot for steel (top) and aluminum (bottom) panels irradiated with an Nd:YAG laser at varying laser fluence and shots per area. The black line shows the baseline contact angle for unirradiated material.

3.1 Excimer-shot samples

Aluminum

First we consider excimer-shot samples. SEM images show the surface topography that resulted in the various surface conditions. Fig. 3 shows a fluence series at constant shot density, akin to taking a horizontal slice across Fig. 1. The images in Fig. 3 were taken at low resolution, and show the large scale features the samples exhibit. At higher resolution (Fig. 4 and Fig. 5), fine features decorating the coarser-scale undulations are visible, becoming larger and more pronounced at higher fluence. The fine features in Fig. 4(b) have a feature width of about $0.3 \mu\text{m}$; in Fig. 4(c), features of about this size decorate larger features of about $1.5 \mu\text{m}$ in width, and by Fig. 4(d), only the large $1.5 \mu\text{m}$ features are evident. Holding the fluence constant and increasing the shot density shows a similar progression, as in Fig. 6; the overall roughness of the surface increases, as does the size of the representative surface features, which grow from about $0.2 \mu\text{m}$ in Fig. 6(a) to about $0.9 \mu\text{m}$ in Fig. 6(d)

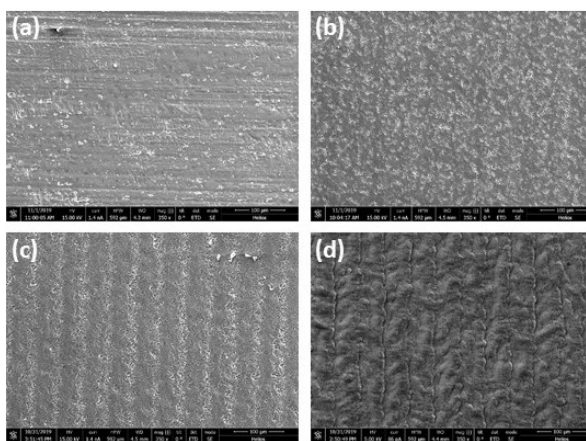


Fig. 3 Excimer-shot Al irradiated with 1500 shots per area at (a) 0.3 J/cm², (b) 1.0 J/cm², (c) 1.5 J/cm² and (d) 3.0 J/cm², all at 350× magnification.

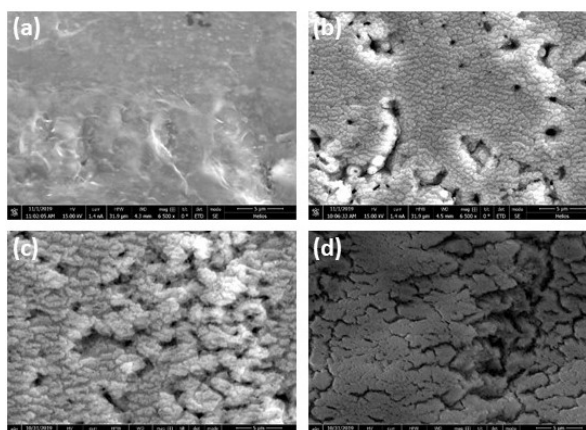


Fig. 4 Excimer-shot Al irradiated with 1500 shots per area at (a) 0.3 J/cm², (b) 1.0 J/cm², (c) 1.5 J/cm² and (d) 3.0 J/cm², all at 6500× magnification.

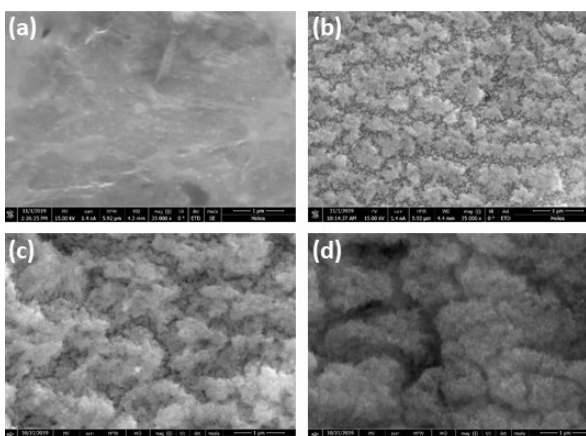


Fig. 5 Excimer-shot Al irradiated with 1000 shots per area at (a) 0.3 J/cm², (b) 1.0 J/cm², (c) 1.5 J/cm² and (d) 3.0 J/cm², all at 35,000× magnification.

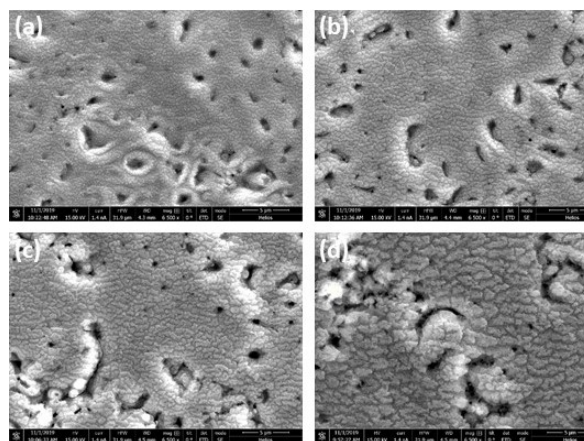


Fig. 6 Excimer-shot Al irradiated at 1 J/cm², with (a) 750, (b) 1000, (c) 1500, and (d) 3000 shots per area, all at 6500× magnification.

Steel

Excimer-shot steel samples show some similarities to the Al samples. Fig. 7 and Fig. 8 show representative images from varying the laser fluence and shot density, respectively. In Fig. 7, the qualitative appearance of the surface topography is dramatically different between the lowest and highest fluence, whereas in Fig. 8, the images are qualitatively similar, with larger undulations decorated by small features, but the length scale increases considerably as the shot density increases. Specifically, in Fig. 8(a), the typical feature is about 0.5 μm in width, whereas in Fig. 8(d) it is 5 μm.

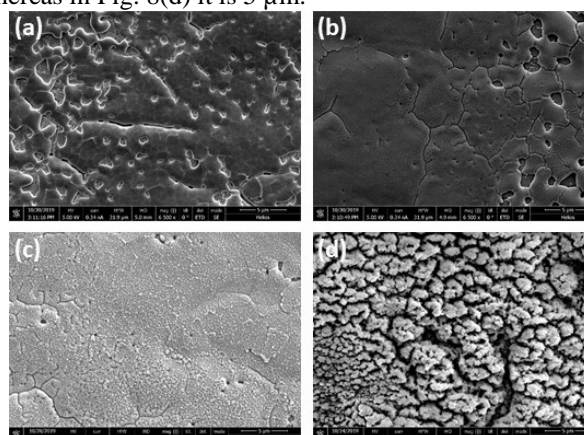


Fig. 7 Excimer-shot steel irradiated with 750 shots per area at (a) 0.3 J/cm², (b) 1.0 J/cm², (c) 1.5 J/cm² and (d) 3.0 J/cm², all at 6500× magnification.

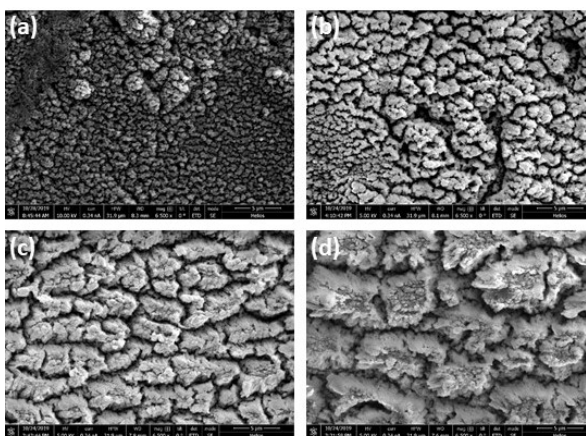


Fig. 8 Excimer-shot steel irradiated at 3 J/cm^2 with (a) 375, (b) 750, (c) 1500 and (d) 3000 shots per area, all at $6500\times$ magnification.

3.2 Nd:YAG-shot samples

Steel

In Fig. 9 and Fig. 10, similar evolutions for Nd:YAG irradiations of steel are presented, varying the shot density and laser fluence, respectively. Although some similar trends are evident, the overall topographic appearance of these samples is quite different from excimer irradiations.

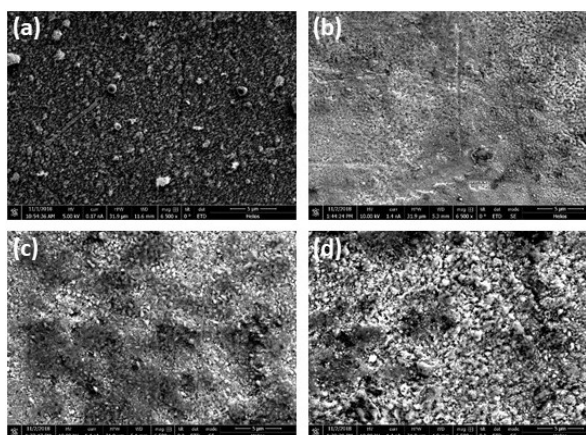


Fig. 9 Nd:YAG-shot steel irradiated at 2.3 J/cm^2 with (a) 80, (b) 120, (c) 310 and (d) 820 shots per area, all at $6500\times$ magnification.

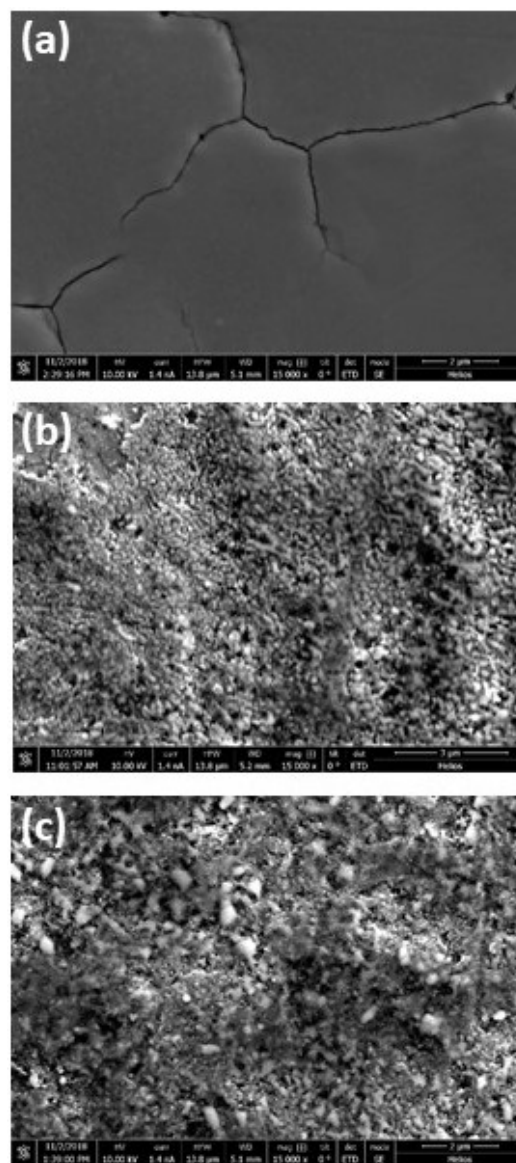


Fig. 10 Nd:YAG-shot steel irradiated with 310 shots per area at (a) 0.27 J/cm^2 , (b) 1.15 J/cm^2 , (c) 2.3 J/cm^2 , all at $15,000\times$ magnification.

Aluminum

In Fig. 11 and 12, a similar progression for Al samples is observed, which like the steel samples, little resembles the progressions for excimer-irradiated samples, even taking into account that the shot densities are lower for the Nd:YAG samples than for most of the excimer samples.

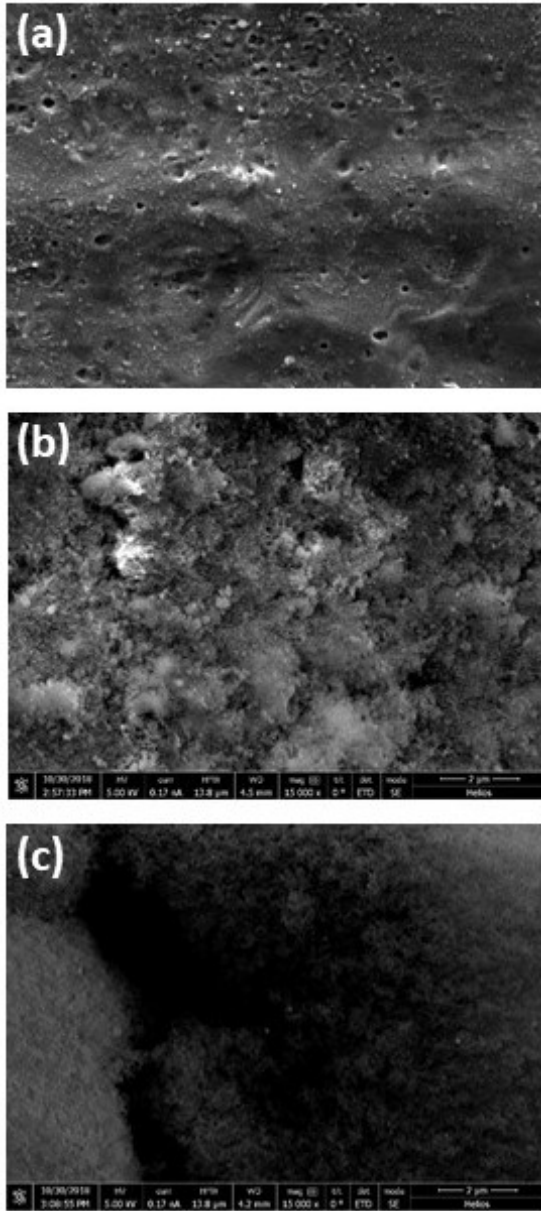


Fig. 11 Nd:YAG-shot Al irradiated with 310 shots per area at (a) 0.27 J/cm², (b) 1.15 J/cm², (c) 2.3 J/cm², all at 6500× magnification.

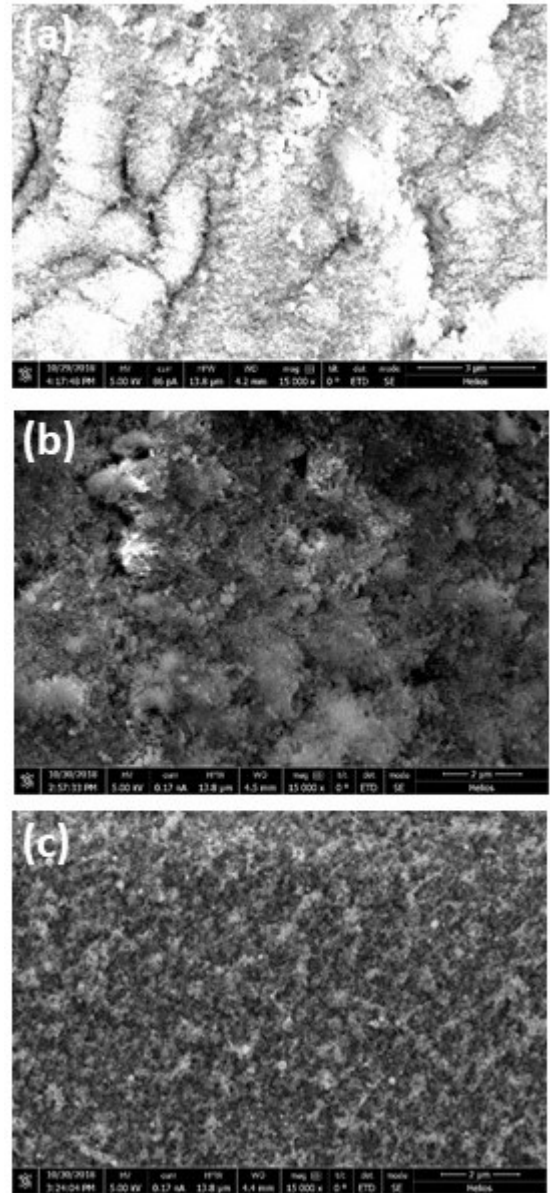


Fig. 12 Nd:YAG-shot Al irradiated at 1.15 J/cm², with (a) 120, (b) 310, and (c) 820 shots per area, all at 6500× magnification.

The range in the degree of overlap between shots is evident in Fig. 13, which shows Al irradiated with the excimer laser at three shot densities. All three show ridges that are parallel to the slow axis, but along the fast axis there is more topography at the lower shot density.

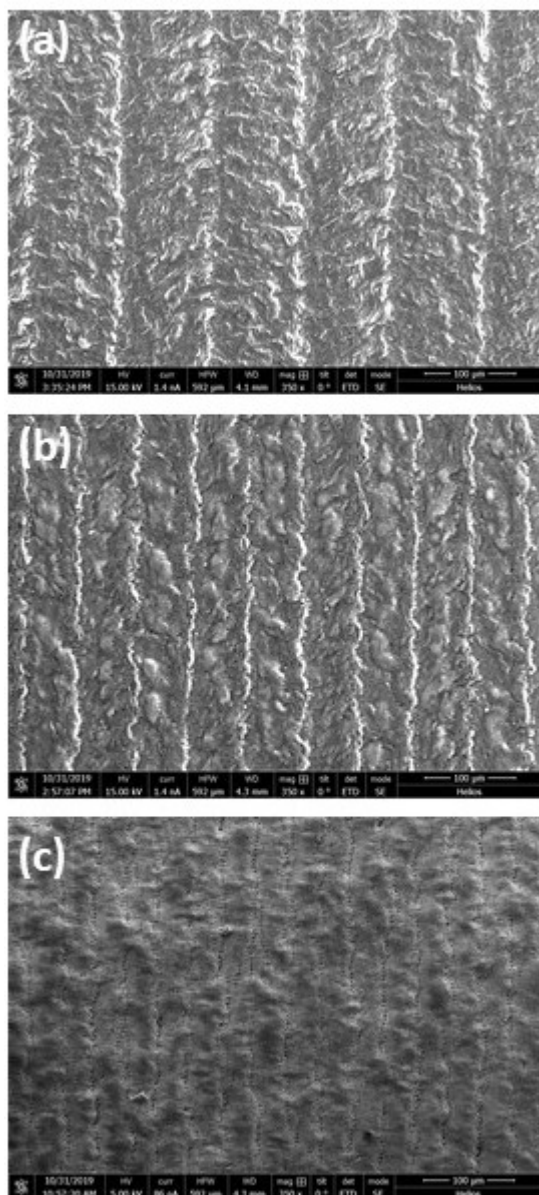


Fig. 13 Excimer-shot Al irradiated at 3.0 J/cm^2 , with (a) 375, (b) 1000, and (c) 3000 shots per area, all at $350\times$ magnification.

4. Discussion

The contact angle data show several noteworthy features, which the microscopy can help interpret.

First, the contact angles of irradiated material show considerable change compared to the unirradiated material. The sample in the lower-left corner of each contour plot received the fewest shots per area and the lowest fluence, and shows the smallest topography change. These samples would be expected to show a contact angle closest to the unirradiated material, and with the exception of excimer-shot steel, which showed a contact angle of 95° compared to 79° for bare steel, this is in fact observed. However, the contact angle deviates considerably from the unshot material as fluence, shot density, or both, are increased. The fact that the lowest fluence and shot density yielded nearly no difference in contact angle suggests that a topographical effect, not a chemical

modification to the surface, dominates the contact angle behavior

Second, the contact angle changes are non-monotonic in both laser fluence and shot density. For almost every fluence and shot density, following a line from low to high results in both increases and decreases in observed contact angle. Moreover, the observed contact angles are sometimes greater and sometimes less than the unirradiated material.

If we draw a horizontal line across the two panels of Fig. 1 at 1500 shots per area, and look at the topography as a function of fluence, the resulting comparisons are shown in Fig. 14 and Fig. 15, for steel and Al, respectively. Both show a progression from a relatively smooth surface, to a surface with some undulations decorated with small-scale roughness, and finally a surface with large-scale features, also decorated with small-scale roughness. The surface of the lowest fluence, despite having some small-scale features, is reasonably smooth and therefore gives a comparable contact angle to the unshot surface. At intermediate fluence, the surface exhibits the two different length scales of roughness characteristic of the Lotus effect^{4,5}, and thus the surface is maximally hydrophobic for this condition. Finally, at high fluence, the large-scale surface so dominates the topography that the hydrophobic effect of the small-scale features is overwhelmed, and thus the surface has become hydrophilic.

Relatedly, Fig. 16 shows four images, in an array that corresponds to the four circles shown in the inset. The 1.5 J/cm^2 , 3000 shots per area sample (top left) and the 3 J/cm^2 , 375 shots per area sample (lower right), have the highest contact angle, and these surfaces are the most similar, showing two length scales of surface roughness, each having a fine scale of roughness on the order of a few hundred nm decorating features with a width of about 1.5 microns. The 1.5 J/cm^2 , 375 shot per area sample also has a high contact angle, but appears to have only a single length scale of surface feature, with features 10s of nm in width. In contrast, the 3 J/cm^2 , 3000 shot per area sample has a lower contact angle than unshot steel, and it has the largest length scale of roughness, with large features $5 \mu\text{m}$ or more in width that the narrowest point. Although its large features are decorated with some bumps several hundred nm in width, the large island features clearly dominate the topography. This image corroborates the interpretation that surfaces with the right kind of surface topography become hydrophobic, while others become more hydrophilic, and that different laser conditions can induce similar surface conditions. Even though the top left and bottom right surface do not look *identical* – clearly these are different surfaces – they are sufficiently comparable with respect to the needed two length-scales of roughness that they produce similar effects when subjected to wetting.

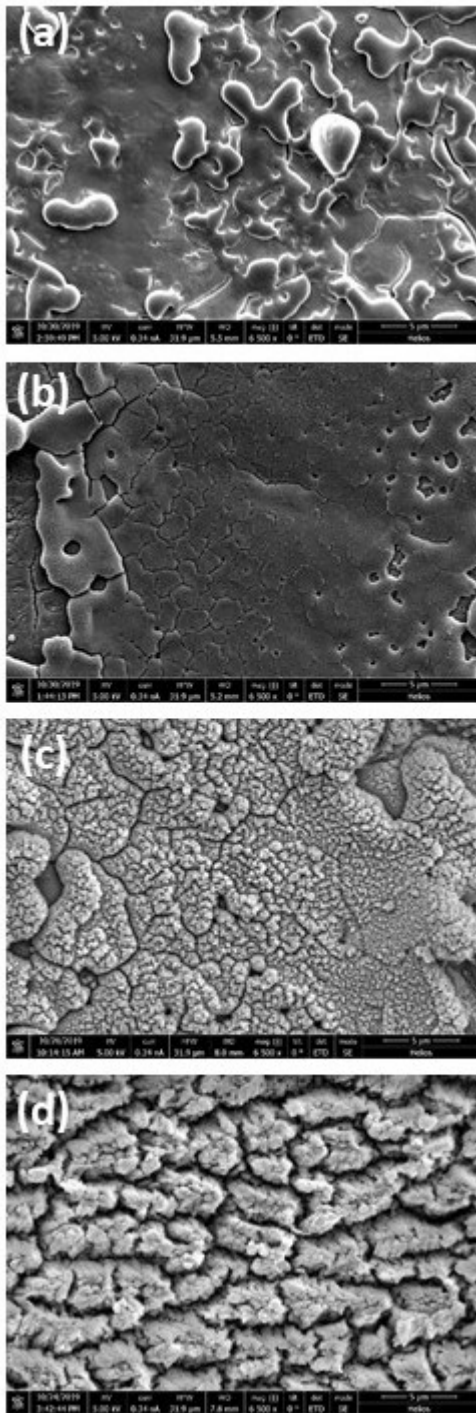


Fig. 14 Excimer-shot steel irradiated with 1500 shots per area at (a) 0.3 J/cm², (b) 1.0 J/cm², (c) 1.5 J/cm² and (d) 3.0 J/cm², all at 6500× magnification.

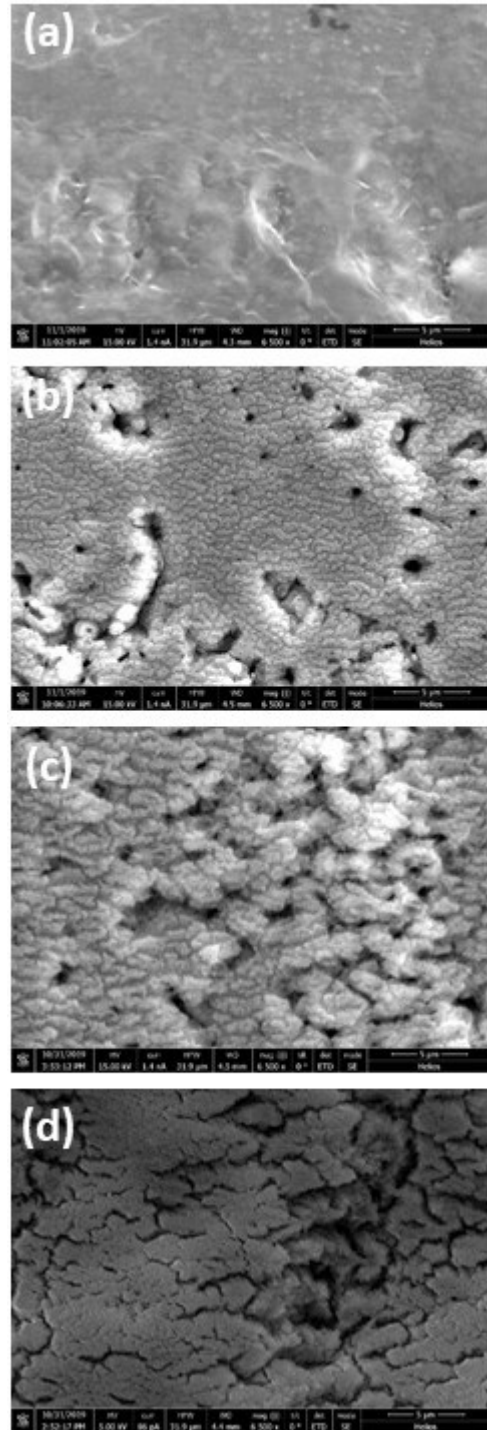


Fig. 15 Excimer-shot Al irradiated with 1500 shots per area at (a) 0.3 J/cm², (b) 1.0 J/cm², (c) 1.5 J/cm² and (d) 3.0 J/cm², all at 6500× magnification.

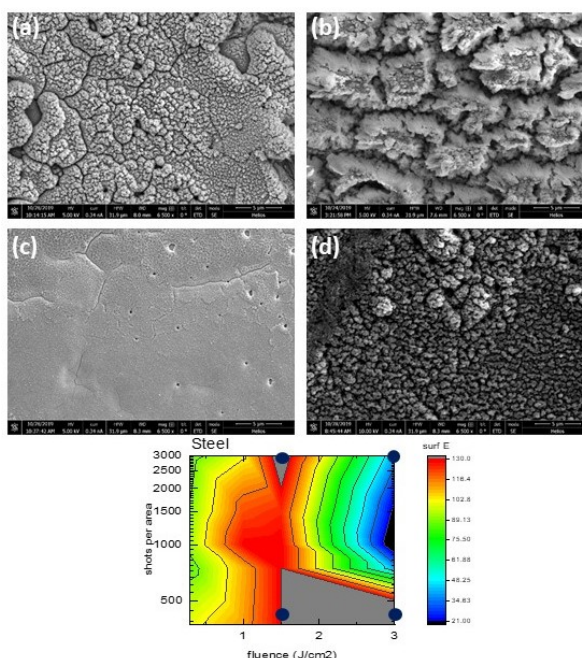


Fig. 16 (a)-(d) Excimer-shot steel, all at 6500 \times magnification. (a) 1.5 J/cm², 3000 shots per area; (b) 3.0 J/cm², 3000 shots per area; (c) 1.5 J/cm², 375 shots per area; (d) 3.0 J/cm², 375 shots per area. Lower panel: contour plot from Fig. 1; dots show the conditions corresponding to the images in (a)-(d).

Third, the surface is more hydrophobic when irradiated with 248 nm (excimer) light than with 532 nm (Nd:YAG) light. Fig. 17 provides some insight into this finding. The top row shows irradiated steel while the bottom row shows irradiated Al; the left shows irradiations at 532 nm and the right at 248 nm. The fluence and shot density are comparable. For both materials, the 532 nm samples are less hydrophobic than unshot material, whereas the 248 nm samples are more hydrophobic than unshot material. Comparing the left and right columns show that the topography is different for the different laser wavelengths. Although the 532 nm samples (left) show significant roughness, this is consistent with a single length scale of roughness, which appears to result in reduced hydrophobicity. In contrast, the 248 nm (right) samples are more consistent with two length scales, although the small-scale roughness of the steel sample is very fine.

An explanation for this discrepancy is not readily available. The skin depth of Al at 248 nm and 532 nm is 0.24 nm and 0.31 nm, respectively. These are so similar, and so short compared to the length scale of the roughness, that it is unlikely that differences in the absorption depth of the light can account for the topographical differences. Another possibility is that the slight pulse duration difference (15 ns for the 248 nm laser vs. 5 ns for the 532 nm laser) could lead to differences. The form this could take might be interaction of the laser beam with the ablation plasma, which is known to occur with ns lasers, and which would be more pronounced in the longer 248 nm pulse. We observed that beam occlusion by the ablation plume significantly changed the surface morphology of polymer composite targets irradiated with

a ms pulse laser.²⁰ In a different study, irradiation by a scanned ns laser of a metal target also showed differences as the scanning speed and pulse energy are varied.²¹ In that case, the laser pulse rate was 200 kHz compared to 10 Hz in the experiments reported here, and so the plume was still present during the arrival of the next pulse. A different study reported that the laser-induced crater changes diameter the more important beam-plume interactions become²², while another showed that beam-plume interactions can reduce the effective pulse energy and duration.²³

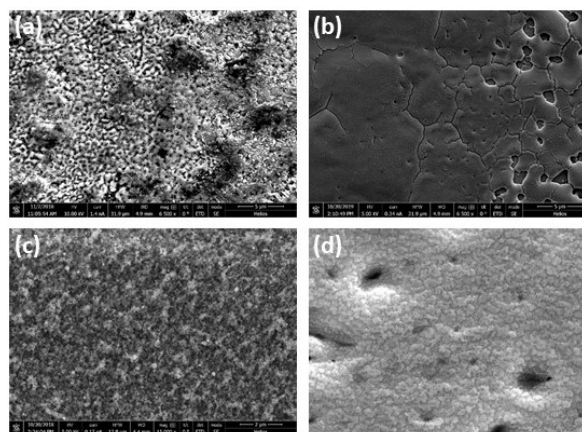


Fig. 17 (a) and (b) steel, (c) and (d) Al. Left side: Nd:YAG at 1.15 J/cm², 820 shots per area. Right side: Excimer at 1.0 J/cm², 750 shots per area. All at 6500 \times magnification.

The best way to investigate whether the pulse duration contributes significantly is to use one of the other harmonics of the Nd:YAG laser, such as 355 nm or 266 nm. Fig. 18 shows a comparison of the surface irradiated by a 355 nm beam (top) with the 248 nm excimer beam (bottom) with all other parameters the same. The length scale of the features for the 355 nm beam is considerably shorter, and is more comparable to that of the 532 nm Nd:YAG samples than to the 248 nm sample in this image. This suggests that the pulse duration, rather than the wavelength, plays the dominant role in setting the length scale of the surface topography.

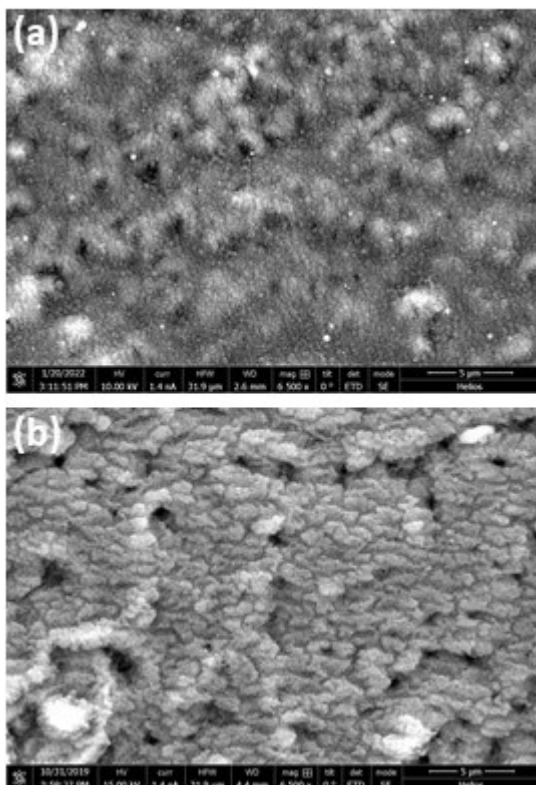


Fig. 18 Aluminum sample irradiated at 1.5 J/cm^2 , 1000 shots per area, with (a) 355 nm and (b) 248 nm beam, both at $6500\times$ magnification.

Reference [21] also notes how the degree of overlap influences the topography of the irradiated area. When there is sufficient overlap between subsequent shots, ablation becomes effectively continuous with a 200 kHz laser. But even with a low-pulse rate laser, the difference between spots that almost entirely overlap and those that only partially overlap can be considerable. In the former case, the centers of the ablation craters are nearly concentric, whereas in the latter case, the center of the ablation craters are far apart, leading to the formation of a ridge between the two adjacent craters.

This phenomenology can be observed in Fig. 13, a high fluence series in which the shot density is varied. At the lowest shot density (375 shots per area), the ridges perpendicular to the slow axis are defined but the curvature of individual spots along the fast axis are also evident. These are less pronounced at intermediate shot density (1000 shots per area) and washed out entirely at high shot density (3000 shots per area). However, the absolute fluence also plays a role in setting the crater depth, as the comparison in Fig. 19 makes clear. The sample in Fig 19(a) was irradiated at a lower fluence, and shows fine-scale particles but no large surface undulations, whereas the sample in Fig 19(b) was irradiated at high fluence and shows larger undulations and larger-scale particles decorating those undulations. Correspondingly the higher-fluence sample (Fig. 19(b)) shows enhanced hydrophobicity whereas the lower fluence sample's hydrophobicity is comparable to untreated Al.

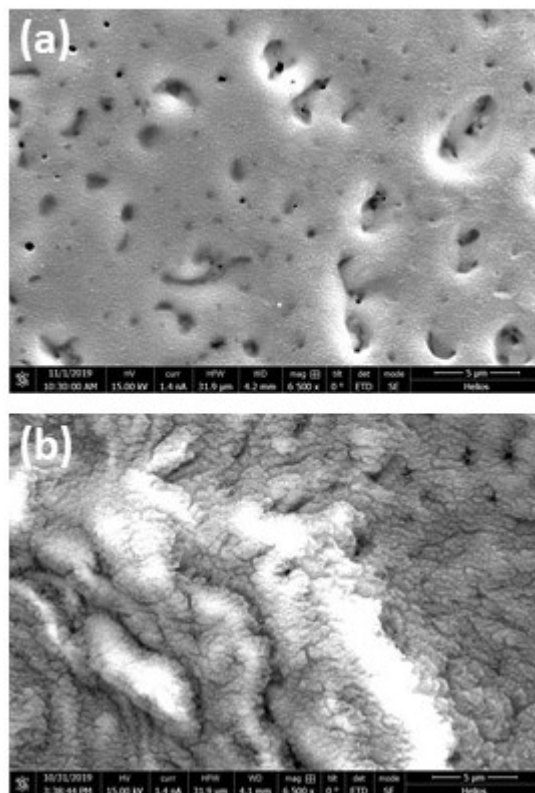


Fig. 19 Excimer-shot Al irradiated with 375 shots per area at (a) 1.0 J/cm^2 and (b) 3.0 J/cm^2 , both at $6500\times$ magnification.

Finally, the surfaces created in this work do not show the order achieved by other fabrication methods, such as the use of an interference pattern beam^{9,14} or the use of a computer-controlled mirror with an f-theta lens.^{24,25} The latter approach, combined with irradiation at an angle, enables the creation of a directionality to the surface, permitting steering of water droplets akin to the performance achieved by shark or snake skin. The surfaces in the present study were not measured with sliding contact angle measurements, but given their relative homogeneous appearance, it is not expected that they would exhibit a directional steering of water droplets. However, as is common knowledge in laser ablation experiments, surface cones tend to emerge in a direction parallel to the incidence angle of the laser beam. Thus, it is possible that a large-spot technique such as the one reported in this paper could produce directional surfaces simply by irradiating the substrate from non-normal incidence. Future work exploring this, as well as making sliding contact angle measurements, could provide interesting insights into the potential range of dynamic hydrophobic surfaces this technique could permit.

5. Conclusion

Aluminum and steel panels were irradiated with nanosecond pulsed lasers at 248 nm and 532 nm at varying shot densities. The surface topography was measured with electron microscopy, and showed combinations of long length scale undulations and ridges and small length scale particles, with the relative amount of each type of feature depending on the laser conditions. Measurements of the contact angle of water showed that some surfaces become

more hydrophobic after irradiation and some became less. There is agreement between the microscopy and surface topography in that surfaces that showed two length scales of roughness were more likely to exhibit enhanced hydrophobicity than those that exhibited only one length scale, consistent with the familiar Lotus effect.

Future work could seek to apply coatings to these surfaces, to ascertain whether the surfaces improve or hinder the coating's ability to bond well to the surface.

Acknowledgement

This project was supported by the Department of Defense's Strategic Environmental Research and Development Program (SERDP).

Disclosure

The author declares no conflicts of interest.

References

- [1] C.-Y. Lee, J.A. McCammon, and P.J. Rossky: *J. Chem. Phys.*, 80, (1984) 4448.
- [2] A. Poynor, L. Hong, I.K. Robinson, S. Granick, Z. Zhang, and P.A. Fenter: *Phys. Rev. Lett.*, 97, (2006) 266101.
- [3] L. Gao and T.J. McCarthy: *J. Am. Chem. Soc.*, 128, (2006) 9052.
- [4] A. Marmur: *Langmuir* 20, (2004) 3517.
- [5] M. Yamamoto, N. Nishikawa, H. Mayama, Y. Nonomura, S. Yokojima, S. Nakamura, and K. Uchida: *Langmuir*, 31, (2015) 7355.
- [6] G.D. Bixler: Ph.D. thesis, The Ohio State University (2013).
- [7] C.H. Crouch, J.E. Carey, J.M. Warrender, M.J. Aziz, E. Mazur, and F.Y. Génin: *Appl. Phys. Lett.*, 84, (2004) 1850.
- [8] I. Etsion: *J. Tribology*, 127, (2005) 248.
- [9] A.S. Sabau, J. Jun, and D. McClurg: *Int. J. Adhesion Adhesives*, 102, (2020) 102641.
- [10] T.T. Wong and G.Y. Liang: *J. Mat. Proc. Tech.*, 63, (1997) 930.
- [11] T.M. Yue, L.J. Yan, C.P. Chan, C.F. Dong, H.C. Man, and G.K.H. Pang: *Surf. Coat. Tech.*, 179, (2004) 158.
- [12] P. Peyre, X. Schepereel, L. Berthe, C. Carboni, R. Fabbro, G. Béranger, and C. Lemaitre: *Mat. Sci. Eng.*, A280, (2000) 294.
- [13] K.G. Watkins, M.A. McMahon and W.M. Steen: *Mat. Sci. Eng.*, A231, (1997) 55.
- [14] J. Jun, A.S. Sabau and M.C. Stephens: *Corrosion Journal*, 77, (2021) 575.
- [15] M. Tang, V. Shim, Z.Y. Pan, Y.S. Choo, and M.H. Hong: *J. Laser Micro/Nanoeng.*, 6, (2011) 6.
- [16] M. Thieme, R. Frenzel, S. Schmidt, F. Simon, A. Hennig, H. Worch, K. Lunkwitz, and D. Scharnweber: *Adv. Eng. Mat.*, 3, (2001) 691.
- [17] A.Y. Vorobyev and C. Guo: *Opt. Express*, 18, (2010) 6455.
- [18] A.Y. Vorobyev and C. Guo: *J. Appl. Phys.*, 117, (2015) 033103.
- [19] J. Yang, J. Lian, Q. Dong. and Z. Guo: *Appl. Surf. Sci.*, 229, (2004) 2.
- [20] S.F. Bartolucci, M.J. Miller, and J.M. Warrender: *J. Appl. Phys.* 120, (2016) 225103.
- [21] J. Yuan, L. Liang, G. Lin, X. Li, and M. Jiang: *Opt. Express* 27, (2019) 23204.
- [22] A. A. Semerok, B. Salle, J.-L. Lacour, J.-F. Wagner, G. Petite, O. Gobert, Meynadier, and M. Perdrix: *Proceedings of SPIE*, 4424 (2001) 574.
- [23] S. Nammi, N.J. Vasa, B. Gurusamy, and A.C. Mathur: *J. Phys. D.: Appl. Phys.*, 50, (2017) 355204.
- [24] Y. Zhao, Y. Su, X. Hou, and M. Hong: *Opto-Electronic Advances*, 4, (2021) 04210008.
- [25] Y. Su, Y. Zhao, S. Jiang, X. Hou, and M. Hong: *Advanced Materials Interfaces*, 8, (2021) 2100555.

(Received: September 2, 2022, Accepted: November 13, 2022)